

Gamma Radiation Studies on Optical Materials

Eric Colby, *Member*, Gary Lum, *Member*, Tomas Plettner and James Spencer, *Member*, *IEEE*

Abstract—Results for the effects of γ_s on materials for a new laser-driven accelerator are presented. Various optical and laser materials are compared. While Si and fused c-SiO₂ appear ideal for sub-bandgap laser wavelengths, other interesting candidates include certain fluorides and compound semiconductors.

Index Terms—lasers; damage; silicon; a,c-silica; impedances; optical/laser materials; transmissive/reflective; III-V; II-VI.

I. INTRODUCTION

ANY number of studies, in various contexts, on the effects of radiation on electronics exist but there are relatively few on the optical properties of interest here where both surface and bulk properties are important. An example is laser damage thresholds as a function of pulse width, polarization, frequency, power and number of pulses as well as its interplay with other sources such as displacement damage. Further, the range of materials studied is typically limited to the obvious ones for space applications e.g. glasses [1], [2] that can be quite sensitive and hard to fully remediate.

Our first accelerator cells [4], [5] were modular and based on high-reflectivity, coated silica. Our ultimate goal is an “accelerator-on-chip” with reflective and transmissive optics in a micromachined, highly repetitive, parallel architecture [6]. Thus, we are pursuing a program whose goal is to understand the sources and types of radiation, their magnitudes, effects and potential mitigations as well as the underlying science. Here, we describe the basic problem and then give our first results and conclusions based on using a single, well-defined source - the Lockheed Martin Co⁶⁰ γ -source.

II. PROBLEMS AND POTENTIAL PAYOFFS

High energy colliders may be the most complex scientific instruments ever built using every form of technology. As for many modern systems, they have grown exponentially [7]. However, in most cases, cost and reliability improved due to reduced size as well as increased production and integration [6]. Although the next generation collider will use conventional RF there is a clear need for new techniques such as lasers provide assuming that adequate materials are available.

These systems and their tensor electron beams suggest many important applications including fast electro-optical switches,

Manuscript received July 16, 2002. This work was supported in part by the U.S. Department of Energy contract DE-AC03-76SF00515.

J. E. Spencer is with the Stanford Linear Accelerator Center, Menlo Park, CA 94205 USA (telephone: 650-926-3385, e-mail: jus@slac.stanford.edu).

E. R. Colby is with the Stanford Linear Accelerator Center, (telephone: 650-926-3709, e-mail: ecolby@slac.stanford.edu).

G. Lum is with Lockheed Martin Space Systems, Sunnyvale, CA 94088, USA (telephone: 408-756-0120, email: gary.lum@lmco.com).

T. Plettner, is at Stanford University, (telephone: 650-218-4814, e-mail: tpletne@stanford.edu).

high density magnetic storage and direct-write, e-beam lithography [6]. Similarly, due to the size and types of materials, one also expects many space applications that are impractical based on current accelerator technology. However, because future colliders require higher energies and luminosity, beams with unprecedented energy densities are required. While such beams should provide many possibilities for frontier physics, they also imply unprecedented containment and damage problems.

Fig. 1 demonstrates the problems and opportunities. Most glasses have complex, compound compositions that are quite susceptible to damage. Varieties tested with 152 MeV protons all showed damage at 10 kRad(Si) [2]. In our first run, a thick, plate-glass sample was irradiated with 42 kGy of gammas that visually blackened it and lowered its transmission spectrum as shown by the lowest curve in Fig. 1. The best we could achieve after many attempts to restore it with UV (broadband photo-bleaching [3]) and thermal anneals typical of those we use for quartz vacuum windows is shown by the middle curve. This material is a better UV/visible filter or detector than a window.

III. BASIC IDEAS AND CHARACTERISTICS

One can understand vacuum laser acceleration consistently for both particles and fields as well as conventional RF even though the conducting waveguides have much higher complex permittivities. Phase space volumes, phase and group velocity, electrical and optical impedances are shared concepts. The limiting factor on the acceleration gradient is the electric field damage threshold of a material. Structures made from dielectric materials are expected to provide an order of magnitude improvement over that achieved with RF but surface and bulk damage now become important because they can modify the breakdown voltages in these regions in different ways.

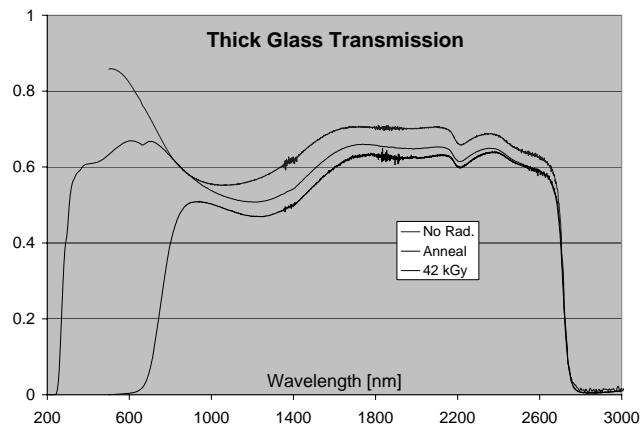


Fig. 1. Transmissivity spectra through 1.1 cm thick plate glass after Co⁶⁰ γ -irradiation. Spectra are stacked according to their order in the insert.

A. Figures-of-Merit (FoM)

While there are many FoMs such as the invariant 6D brightness useful for applications such as e-beam lithography, we will discuss only those useful for damage considerations. Near the detector, showers from radiative Bhabhas damage permanent magnets and detector components and monitors and their rate is directly proportional to the luminosity. Likewise, impedances relate directly to aging and damage effects such as heating due to absorption and low thermal conductivity.

1) *Luminosity*: The most important figure-of-merit is the usable luminosity. The generalized luminosity[8], [9] was based on the observation that **all** colliding beam machines as well as **all** incident channels in any particular collider can be expected to have a luminosity proportional to the square of the *primary*, incident bunch ‘charge’ N_B^2 or some equivalent thereof that can be brought into collision per unit time within an effective area that contains the *effective* number \tilde{N}_B based on conversion efficiencies and detector constraints[8], [9], [10].

For a laser driven accelerator, when the laser and e-beam normalized emittances are matched, one can write, in terms of the standard expression,

$$\mathcal{L} = \frac{f_T n_B N_B^2 H_D}{4\pi\sigma_x^* \sigma_y^*} \zeta \rightarrow \frac{f_T n_B N_B^2 \gamma H_D}{4\pi\epsilon_n \beta^*} \zeta \propto \frac{P_b}{\lambda Z_R} N_B H_D \zeta \quad (1)$$

where the parameters are the usual ones[8], [9], [10] e.g. $\sigma_{x,y}^*$ is the undisrupted, rms spot size at the interaction point (IP) and β^* is the magneto-optical ‘depth-of-field’ at the IP. The arrow simplifies to round beams and $P_b \propto f n N E_b$ is the incident, primary electron beam power. H_D is a pinch enhancement factor of order unity. β^* is equivalent to the Rayleigh range $Z_R > \lambda$, the laser wavelength. In this scenario, luminosity increases with decreasing λ^2 .

2) *Impedances*: One sees that \mathcal{L} is proportional to the power available to accelerate the primary beam. The on-axis, unloaded gradient of an accelerator cell can be defined as

$$G_U = \frac{\sqrt{P Z_c}}{\lambda} \stackrel{1.5\mu\text{m}}{\rightarrow} G_U [\text{MeV}/\text{m}] = \sqrt{P [\text{W}]} \quad (2)$$

for $Z_c \equiv 2.25\Omega$. Equation 2 defines the characteristic impedance of a structure’s accelerating mode. Z_c can vary greatly but 2.25Ω is reasonable. The peak power¹ is determined by the structure’s damage threshold. Dielectrics such as fused silica allow 1-2 J/cm²[11] in the near IR below 10 ps pulse widths as discussed later and shown in Table I. Commercial sources[12] are available that can provide 50 MHz rep-rates as compared to typical RF rep rates of 120 Hz.

This expression implies shorter wavelengths are preferred over power or impedance but if power or efficiency was not a problem we could get any \mathcal{L} we could use. Any choice of λ assumes that one has the power source and the means to fabricate structures to the required tolerances that can withstand the power at that wavelength. With the rapid development of high power lasers and micromachining techniques we have a good justification for LEAP[5] with good materials science.

If we assume that a fixed power is available, we can enhance Z_c by series addition of cells to improve energy gain per unit power by $\sqrt{n_c}$

¹Note that a μJ in a ps gives 1 GeV/m - ten times better than RF.

$$E_b = \sum_{n_c} \frac{l_c}{\lambda} \sqrt{\frac{P}{n_c}} Z_c = l_c \sqrt{n_c} G_U. \quad (3)$$

l_c is the acceptable slippage distance between bunchlet and wavelet $l_c \leq \lambda/2(1-\beta)$. This increases the length and it is clear that adding cells in parallel[9] can reduce it. The impedance of this parallel path Z_T for a wavelet determines the so-called shunt impedance as well as the allowable number of parallel bunchlets. It is determined by Z_c and the transmittance $T(\lambda)$ of the structure between cells. As will be shown, T can be large for silicon (or silica) for laser wavelengths $\lambda > 1.2\mu\text{m}$ when we couple the wavelets into these materials properly.

The beam excites higher modes that dissipate energy and this provides another impedance Z_h that leads to a loaded gradient G_L that is not less than half G_U but depends on the charge per bunchlet. This is a justification for tensor beams that can reduce this charge. Clearly, we want to increase Z_c , reduce Z_h and maximize T .

B. Dielectric loaded waveguide/accelerator

Whether one has a disc or dielectric loaded guide structure, the modes can be classified as transverse magnetic TM_{klm} with $E_z \neq 0$ and $B_z \equiv 0$ and p polarized wavelets for cylindrical symmetry. For waves of finite extent, the group velocity in any direction is $v_g < c$. From the waveguide dispersion equation or geometric arguments one then has, above cutoff,

$$\beta_g = \frac{v_g}{c} = \sqrt{1 - \left(\frac{\nu_c}{\nu}\right)^2} = \frac{c}{v_p} \ni v_g v_p = \frac{c^2}{n^2} = \frac{1}{\epsilon\mu}. \quad (4)$$

The index n is generally complex and the cutoff frequency ν_c results from the waveguide’s cross section e.g.

$$\nu_c = c \sqrt{\left(\frac{k}{2a}\right)^2 + \left(\frac{l}{2b}\right)^2} \quad (5)$$

for a rectangular guide. Note that the mode’s unloaded, lossless wave impedance $Z_{\text{TM}} = (E/H)_{xy} = \beta_g Z_0$. We want v_p close to c i.e. $\nu \gg \nu_c$ because this increases the slippage distance or guide length. For high enough energies:

$$v_p/c = \lambda_{wg}/\lambda = \sqrt{\frac{1}{1 - (\lambda/\lambda_c)^2}} \leq \gamma^2. \quad (6)$$

This ratio is determined by varying the cell length for a given laser λ , aperture and crossing angle to optimize gain. One concludes that we must either increase λ_c i.e. the guide size or decrease λ - neither of which is very agreeable except for the large changes achievable with lasers.

An old idea is to load the waveguide with dielectric. For small apertures:

$$v_p/c = \lambda_{wg}/\lambda = \sqrt{\frac{1}{\epsilon_r \mu_r - (\lambda/\lambda_c)^2}} \leq \gamma^2. \quad (7)$$

This expression suggests a graded index and shows why a laser accelerator is possible. Increasing ϵ_r or μ_r from vacuum values provides knobs that allow smaller waveguides and higher accelerating fields. Problems include variable capacitance through charge buildup from lost electrons, dielectric breakdown and aging from poor heat dissipation or radiation damage.

IV. IMPORTANCE OF REFLECTANCE AND TRANSMITTANCE

In contrast to RF approaches, the reflectance, transmittance and absorptance, with $R + T + A = 1$, are important to every part of our problem. Thus, the expressions above are valid and, in a geometric picture, can be thought of as defining the mean angle of propagation of the fundamental mode down the guide i.e. $\beta_g \equiv \cos\theta_c$. For conventional metallic guides, the characteristic angle $\theta_c = 90^\circ$ defines the cutoff frequency where there is no propagation down the guide. For consistency with optical conventions, we rotate our angle by 90° so normal incidence, defining $k_\perp \equiv k$, now occurs at 0° .

Brewster's angle $\theta_B > 52^\circ$ for the wavelengths and dielectrics or semiconductors of interest here so this angle defines the onset of the parallel, transmission mode while R and the number of reflections per unit length determines the extinction rate of the serial, reflective mode for smaller angles and thereby the serial shunt impedance Z_R as opposed to Z_T mentioned earlier.

Dielectrics have nearly zero absorptance while metals always have greater than zero. Polished metals thicker than ≈ 50 nm can have high reflectances up to 98% at normal incidence while uncoated dielectrics such as glass typically have 4-8%. One quarter-wave layer of intermediate index material can reduce this to $< 1\%$. This is an example of impedance matching where R results from a mismatch. It depends on the materials, angle of incidence, polarization, surface structure and incident intensity.

V. DAMAGE MECHANISMS

In our damage studies, we scan light of variable frequency ω at normal incidence on flat polished surfaces and measure R and T for materials of thickness l subjected to increasing intensities I_k or doses D_l of γ s or neutrons. The first order or infinite half-plane reflectivity, analogous to a transmission line with lossy termination Z_2 , is:

$$R = \frac{(Z_2 - Z_1)(Z_2 - Z_1)^*}{(Z_2 + Z_1)(Z_2 + Z_1)^*} \xrightarrow{0^\circ} \frac{|(n_2 - n_1)|^2}{|(n_2 + n_1)|^2}. \quad (8)$$

Generally, R and T are functions of the variables ω , l , θ , P , ϵ_j , μ_j , I_k , E_{BG} , D_l , t with P the wavelet polarization, E_G the bandgap energy and $Z_j(\omega) \equiv (\mu_j/\epsilon_j)^{1/2}$ the complex wave impedance. The transmissivity, to all orders, is then:

$$T = \frac{(1 - R)^2 e^{-\alpha l}}{1 - R^2 e^{-2\alpha l}} \quad (9)$$

where the complex "index" in (8) is:

$$n_j(\omega) \equiv \sqrt{\mu_{rj}\epsilon_{rj}} = n_{0j}(\omega) + ik_{0j}(\omega) + n_{2j}(\omega)I(\omega) + \dots \quad (10)$$

and $n_{0j}(\omega)$ is the index of refraction that determines the phase (and group) velocities (4) and $k_{0j}(\omega)$ is the extinction index that determines the absorption coefficient $\alpha_j(\omega)$:

$$\frac{T(l)}{T(0)} \approx e^{-\alpha_j l} \quad \text{with} \quad \alpha_j = 4\pi\nu k_{0j}. \quad (11)$$

Frequency ν is in wavenumbers. k_0 relates to conductivity so it is negligible for dielectrics in the visible and near infrared except near strong vibrational bands. Also, for semiconductors below bandgap e.g. standard grade Si [13], one has $k_0 \ll 10^{-5}$ until multi-phonon absorption picks up below 1200 cm^{-1} .

The Sellmeier model describes resonant, nonlinear variations of $n_{0j}(\lambda)$ with λ over this region as well as the dispersion $dn_{0j}/d\lambda$ discussed later. The sign and magnitude of the leading nonlinear term with field strength, n_{2j} , leads to variable lensing action. Such terms produce laser damage through multiphoton excitation and ionization processes $q\hbar\omega \geq E_G$ or self focusing effects[14] that increase the effective intensity I . Samples of the same materials were used to measure, independently, the onset of laser and γ damage with some typical results shown in Table I and Fig's. [2] and [3]. All oxides and no fluorides showed changes between the air and vacuum laser tests.

TABLE I

REPRESENTATIVE MATERIALS AND MEASUREMENTS AT NORMAL INCIDENCE. LASER WAVELENGTH $\lambda=800$ NM WITH 150 FS PULSE DURATION AND $13 \mu\text{M}$ SPOT SIZE. LM1 IS LOCKHEED DOSE #1.

Material Type	Threshold [J/cm ²]		γ -Dose [kGy]				
	Air	Vacuum	LM1	LM2	LM3	LM4	LM5
a-SiO ₂	2.03	1.80	50	62	67	134	60
Al ₂ O ₃	1.57	1.15	45	63	61	139	
HR(800)	0.77	0.77	49	72	59	134	64
LiNbO ₃	0.50	0.19	46	67	63	141	

Radiation damage is specific to the type of radiation and the integrated dose. Materials age, damage, anneal, relax, absorb or adsorb other materials in ways that can seriously change their properties in time dependent ways. Such changes can show a strong frequency dependence as when hydrogen diffuses into or out of silica or the growth of color centers from point defects.

Such defects can be vacancies, substitutional dopants or impurities, substitutional interstitials or impurities that migrate. These are important because they behave differently in amorphous and crystalline materials as well as metals and oxides. In oxides, they are often charged which can lead to significant changes in light transmission. In some semiconductors, we have also seen these effects in the bulk transmission due to intentional doping that can have significant concentrations and can be both charged and neutral. Undoped, thick Si can have observably better transmission than typical Si wafers.

VI. CHOICE OF RADIATION SOURCE

The types of dose and their magnitudes in a collider depend on the subsystem and the location within the subsystem. Typically, in descending order come the beam dumps, the positron target, the damping rings, the accelerator, the detectors and the electron source. Of all of these, the source is the lowest energy and of most interest for practical applications.

Because most source implementations (including ours) involve only low energy electrons, x-rays and gammas ($E < 10$ MeV) we chose the Lockheed Martin Co⁶⁰ γ -source for two reasons. First, it is well calibrated with a well-defined isoradiation grid that allows irradiating many samples simultaneously. More importantly, it provides an average γ energy of 1.25 MeV whose stopping power is *equivalent* to ≈ 600 keV electrons[15]. In fact, the LET is rather flat for electrons from 200 keV-20 MeV. Thus, it is an ideal source to study materials for this important system that will necessarily use many of the same materials as the accelerator and detectors[6].

VII. EXPERIMENTAL SETUP AND PROCEDURES

We used a Hitachi U-4001 spectrophotometer to obtain spectra for various conditions over a wavelength range from $200 \leq \lambda(\text{nm}) \leq 3200$. Due to water absorption bands near 1400, 1900 and 2700 nm, we purged the system with dry air and maintained a positive flow during measurements. One still sees occasional fluctuations in these regions (see Fig. 1) that can be due to changes in surface moisture or when running for extended periods. Baseline scans are necessary for this and to match different sources and detectors over the range that spans the near-UV, visible and near-IR.

Widely different shapes and sizes of samples complicated the situation but they all had polished, parallel entrance and exit surfaces. We used perpendicular entrance angles that were good to a degree or better between the different irradiations for which the relative calibrations were on the order of 0.5 % based on using calibration samples and running sample-free scans against our baseline before and after measuring each batch of irradiations. All irradiations and their subsequent measurements were done at room temperature on samples that were “encapsulated” when not undergoing measurements.

The scan rate, range, resolution and step size were all varied for effect as well as for the material being scanned e.g. the high reflector coatings and laser rods were run at both low and high resolutions down to 1 nm steps. The lowest wavelength accuracy of the instrument was ≈ 1 nm at the longest wavelengths. The shortest wavelength was set to include the 4th harmonic of Nd:YAG at 266 nm although we would have liked to include the VUV down to 100 nm and the mid-IR through 14000 nm because longer wavelength, higher-power, stable lasers would simplify our particular application. Having the higher ranges available also simplifies the assignment of contaminant lines.

After our last irradiations, we obtained access to an IFS 66v/S Bruker FTIR spectrophotometer that allowed overlapping measurements up to $10 \mu\text{m}$. Due to strong water absorption above 4-5 μm , this system operates under vacuum which is an important improvement for nearby, weak absorption lines.

VIII. MEASUREMENT RESULTS

A. Amorphous materials

Amorphous, fused silica (a-SiO₂) is an ideal example whose properties support many applications. It was used for our first accelerator cells due to its good thermal stability that provides stable, high-reflector coatings under high power beams. Because it has a high bandpass for our nominal wavelength range, it has many uses that make its transmission characteristics and their stability important. Fig. 2 shows the transmission spectra, in 1 nm steps, for an uncoated, polished accelerator cell from CVI Laser[16] as a function of total γ -dose in Si equivalents.

The maximum transmission here is $T \approx 95\%$ at 1600 nm. There are four prominent absorption regions near 210, 1385, 2210 and 2760 nm or in frequency: 47,620, 7,220, 4,524 and $3,622 \text{ cm}^{-1}$. The most interesting of these is the activation dip at 212 nm (5.84 eV) where significant damage appears but it is well below any laser wavelength λ_L of interest here except for the 4th harmonic of Nd:YAG where it may be useful for our electron source[6].

Because of its high energy and the fact that the band gap for pure SiO₂ (defect-free quartz or amorphous) is $E_G > 8 \text{ eV}$ (155 nm), this results from electronic excitation of impurities or lattice defects. The ionization potential (IP) of free Al is 5.98 eV or 207 nm but this can't explain the result without creation of additional stable defects of comparable energy because of the strength of the effect. Because the silica[16] is of Type-III, its largest metallic component is expected to be Al (10-20 PPM) which we will see is too small. Although it has the potential for far more Cl, the ionization potential ($\approx 13 \text{ eV}$) is too high to be relevant and HCl vibrations are too low. We know of no other nearby electronic excitations except Na at 5.14 eV (241 nm). It is present in the few PPM range and helps explain the nearby transmission shoulder.

Similarly, we note that free Si has an $\text{IP} \approx 8.2 \text{ eV}$ but has a 3p-3d transition at 221 nm. E' defects[1] related to oxygen vacancies with an electron trapped in the 3p orbital of a Si-Si bond provides a stable defect(hole). Since this can be produced with 1 MeV photons from secondary Comptons this can explain the effect. The observed damage is linear with dose:

$$T(212 \text{ nm}) = 0.823 - 1.36 \cdot \text{Dose}(\text{MGy}) \quad (12)$$

although it is barely visible at low doses for neutrons or γ 's. Increasing the dose would allow us to determine whether the effect saturates as observed for the fused quartz wafer.

The dominant excitation near 2760 nm is often observed. We interpret it as a combination of water and a two-dimensional stretching mode associated with OH that is typically[16] at 1000 PPM. The line at 1385 nm reinforces this assignment by its interpretation as the first harmonic. The small modulation near 900 nm increases with total dose and is the second harmonic with evidence for higher harmonics in the subsequent falloff near 670 nm. This is a good indication of broken SiO₂ bonds that are subsequently passivated by H to form Si-O-H consistent with the fact that this is energetically more stable than water: $\text{H}_2\text{O} + \text{Si-O-Si-} \rightarrow 2(-\text{SiOH})$ and molecular hydrogen[18]. While we have seen evidence for growth of Non Bridging Oxygen Hole defects (NBOH) near 670 nm[19] in both SiO₂ and Al₂O₃, that has no water lines, we saw no obvious growth at 1385 nm. This may be due to migration loss of the cracked hydrogen or a surface related effect.

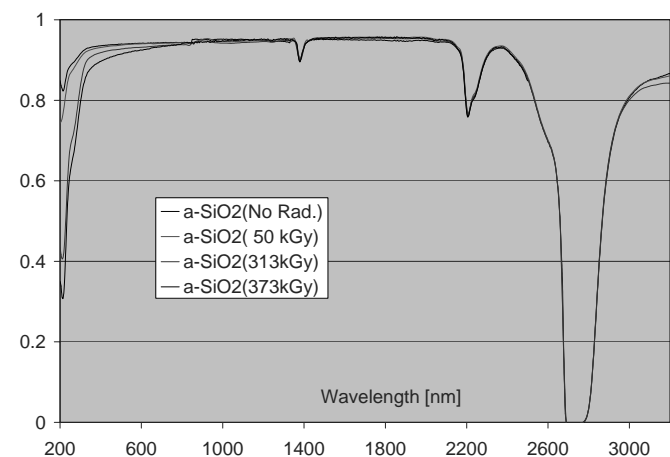


Fig. 2. Transmission spectra through a 6.35 mm thick, polished, silica cell as a function of integrated dose (Si). Spectra are stacked according to insert order.

The remaining region around 2200 nm is two or more lines, as is the strong excitation around 2760 nm with a weak water band evident at 2600 nm (Fig. 1 also). It is important to note that water has symmetric and antisymmetric stretching modes near 3650 and 3760 cm^{-1} with the latter (2660 nm) the stronger. The difficulty in the 2200 nm region is that it could be related to harmonics of unobserved, lower lying levels. The simplest interpretation is that it results from H_2 vibrations because of its energy. The near degeneracy could relate to passivation of O vacancies or substitution impurities in the form of Si-H H-Si or Si-H₂-Si. Alternatively, one knows that CH_4 and CO (also H_2) are hard to remove from processes even under UHV pumping at 10^{-10} Torr. While it is difficult to deal with harmonics or coupled bands, one might assign these lines to harmonics related to vibrations of CO and a triple bond of CO. The spectral transmission of CO_2 matches the profile from 2-3 μm very nicely but there is no evidence for carbon in silica. We will discuss this in more detail by comparison to crystalline SiO_2 , Si and Lithosil[17] that has extremely small metallic impurities.

A discussion[20] of hydrogen defects in a- SiO_2 shows the difficulty arising in understanding amorphous materials and helps to explain the lack of systematic characterizations that provide more direct predictive power for glasses.

The results for a- SiO_2 apply to many substrates insofar as transmission is concerned as shown for a high reflector coating (HR) in Fig. 3. This is intended for use in the Ti:Sa region but is not the same silica material used for Fig. 2 because of the cell's shape. The sharpness of the primary reflection band and the surrounding oscillations result from multi-layer coatings with quarter wave optical thickness $l = \lambda/4n_{0c}$ on a substrate with $n_{0s} < n_{0c}$ based on phase changes $\delta = 2\pi ln_{0c}/\lambda$ for incident light with wavelength λ at normal incidence and a π phase change on reflection at the n_{0s}, n_{0c} interface.

Previous lines, observed at longer wavelengths in Fig. 2, are interspersed with different orders about the primary near $\lambda=800$ nm. Because the light was incident on the substrate side in these two runs, the peak transmission (modulated) is similar to Fig. 2 and shows that k_{0s} is negligible except near the absorption bands that act as bandpass filters. The dispersion increases dramatically at the shorter λ 's (Fig. 10). No damage was observed in the coating up to 378 kGy.

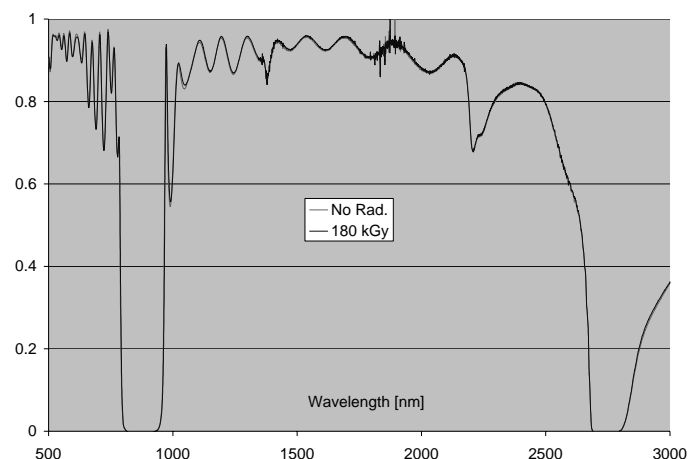


Fig. 3. Transmission spectra through a high reflector (HR) coating on silica for use with Ti:Sa systems as a function of integrated dose (Si). See Table I.

B. Crystalline materials

Examples for crystalline data are shown in Fig. 4 for comparable thickness wafers of quartz (c- SiO_2) and silicon. There is no evidence for damage in any Si sample up to 9 mm for γ -doses up to 370 kGy. Similarly, there is virtually no damage to the quartz except in the near-UV below 300 nm. Contrary to the amorphous silica (a- SiO_2) in Fig. 2, the damage in quartz appears to saturate. Up to ≈ 300 kGy, it grew more slowly at a rate:

$$T(212) \text{ nm} = 0.908 - 0.539 \cdot \text{Dose}(\text{MGy}) \quad (13)$$

or $< 40\%$. There is less water in the quartz which indicates the possibility of fewer O vacancies that can be passivated. Using the Lambert-Beer law we can estimate vacancy concentration:

$$C(\text{PPM}) = \frac{100}{t(\text{cm})} \log_{10}\left(\frac{T_i}{T_o}\right) \approx 150 \quad (14)$$

where t is the thickness of the sample. This is consistent with the expected water content in the a-silica in Fig. 2.

Based on these results, it appears that both Si ($\lambda_L > 1.2 \mu\text{m}$) and fused c- SiO_2 ($\lambda_L > 0.3 \mu\text{m}$) are adequate with certain caveats for the quartz but that quartz is clearly preferable to fused a- SiO_2 for longer wavelengths.

It is useful to study other groups in the Periodic Table as well as hybrid combinations within a group. SiGe and SiC are examples of substitution elements from the same group. SiC has better mobility, bandgap (3.26 eV), breakdown voltage and thermal conductivity than Si. We also explored both synthetic and natural diamond. The two samples that we studied had such poor transmission over the whole range that we could say nothing about the radiation damage. The natural diamond had many defects, presumably from natural radiation damage. This makes it useful as a detector but not for our applications.

With proper doping, good III-V GaAs and II-VI ZnSe give good semiconductor lasers. Fig. 5 shows a thick sample of GaAs that is compared to an undoped, 320 μm , (110)-wafer that is especially interesting for micromachining tests. GaAs (1.42 eV) is easier to do laser damage tests on than Si (1.12 eV) because of its higher bandgap that allows use of the Nd:YAG fundamental but not the Ti:Sa that was used for the laser damage measurements in Table I.

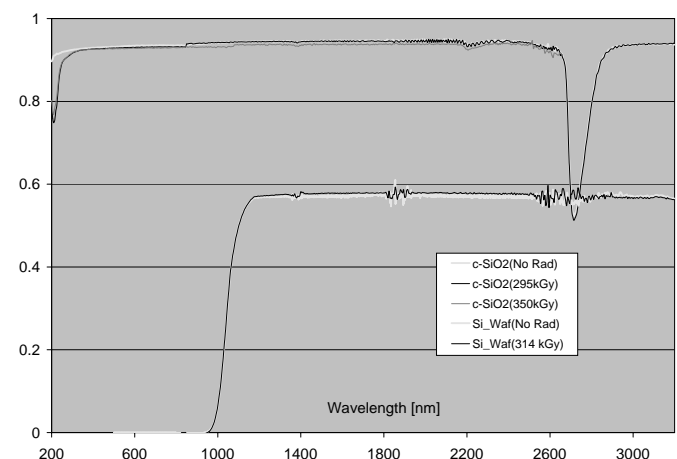


Fig. 4. Transmission spectra through 500 μm wafers of Quartz (upper group of curves) and Silicon (lower group) as a function of integrated dose (Si).

Although the refractive index for GaAs is comparable to Si, it has a much higher extinction index and dispersion (Fig. 10) as well as a much lower thermal conductivity. Although both GaAs samples were undoped, they are still too dissimilar to analyze for the complex, nonlinear index (10). Surface water bands appear more pronounced for the wafers of both GaAs and Si and both materials show serious differences between thick and thin samples possibly due to trapped defects from different anneal cycles during fabrication.

C. Some further silicon comparisons

Considering the lack of significant damage observed in some materials it was thought important to extend the range to get a better idea of the wavelengths accessible to a laser accelerator on the assumption that high power lasers at longer wavelengths could be developed if the material studies supported it. Because we observed no radiation damage in any thickness of Si that we tested up to 3200 nm, measurements were extended using the Bruker system at Stanford's Hansen Experimental Physics Laboratory. Fig. 6 shows the results up to 10 μm in the vicinity of CO₂ lasers. We note that Si is not disadvantaged by a lower transmission for perpendicular incidence since one can couple the light in at the more oblique Brewster angle.

Whereas, the Si wafer showed only modest absorption near 9080 nm, the 9 mm thick Si fell to zero there with several other distinct lines appearing at 7000 nm (6958, 7324 and 7762 nm) and one other stronger band above 10 μm . The data in Fig. 6 shows the difficulty in making generalizations[13] although the thick sample does show a measurable extinction coefficient over the lower half of the plot. If we take the complex index (10) as the same for both Si samples, then from (11) we can eliminate R and n_{0j} , assuming k_{0j} is small, giving:

$$\frac{T(\text{thin})}{T(\text{thick})} \approx e^{\alpha(l(\text{thick})-l(\text{thin}))}. \quad (15)$$

From 1.5-2.1 μm in Fig. 6, this gives $k=(0.74 \pm 0.08) \cdot 10^{-6}$ for silicon so the extinction index is small as assumed.

Because most metallic and non-metallic materials absorb strongly in this region while water is quite transparent above

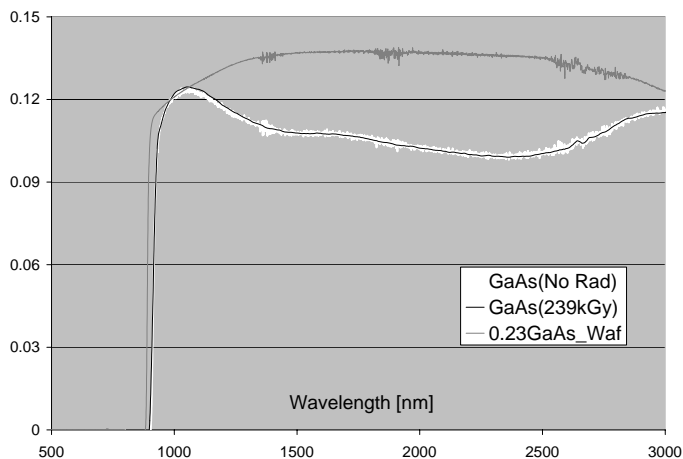


Fig. 5. Transmission spectra through a thin wafer and a thick (6.35 mm) GaAs sample as a function of integrated dose (Si). The wafer was scaled downwards by 0.23 for better comparison. Both samples are undoped.

8 μm , Fig. 6 argues against using CO₂ lasers with Si even though longer wavelengths are needed as discussed later.

However, beginning around 4.5 μm , water absorbs strongly up to 7 μm . As a result, the transmission for the a-SiO₂ cell went essentially to zero and stayed there above 4400 nm with lines near 3800, 4150 and 4400 nm observable. These same lines are seen in the quartz with a 4450 line strongest. This is consistent with the existence of ionic molecules of H₂⁺. Finally, there were observable lines in both SiO₂ samples near 3100 and 3200 nm that were not seen with the Hitachi instrument.

D. Laser and electro-optic materials

Important laser crystals of particular concern were Ti:Sa and Nd:YAG because they are the most widely used for high-power applications in the near IR. Sapphire is a synthetic, hexagonal crystal of aluminum oxide (Al₂O₃). YAG is a cubic crystal of yttrium aluminum garnet (Y₃Al₅O₁₂) with little absorption from 2-3 μm so there was hope that it could withstand the radiation better than other hosts such as glass. Both have a broader transmission bandwidth than a-SiO₂ and the sapphire, although birefringent, showed no radiation damage up to 300 kGy.

We use Ce:YAG for our fluorescent screens that tolerate full electron beam with no apparent degradation. We obtained a variant of Nd:YAG from Lightwave with 1 % Nd, 0.5 % Cr. Fig. 7 compares spectra before irradiation. The Cr³⁺ rod is 2.5 cm long by 0.635 cm diameter. The high purity 1 % Nd³⁺, from VLOC, is 10.2 cm long with polished sides and AR/AR faces. Major differences occur in the short wavelength region.

After only a minor irradiation, comparable to the glass in Fig. 1, there were obvious visual changes in the Nd:YAG that grew worse with dose as shown in Fig. 8. Although the rod was uniformly irradiated over its full length, considerably less damage occurred than for a thin sample [21] whose characteristics matched. This is presumably due to fewer defects based on better crystal fabrication and doping techniques e.g. compare the unirradiated samples here with those in [21]. This was one reason for obtaining the Cr variant shown in Fig. 9. In all cases, our results indicate a greater hardness to higher doses due to both dopant as well as purity, production and doping procedures.

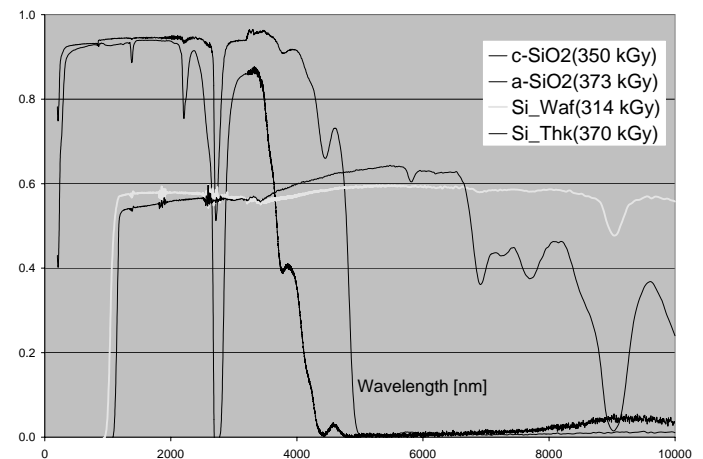


Fig. 6. Comparison of spectra from 0.20-10 μm for different forms of Si in Si equivalent dose. Spectra were taken on two different systems and matched at 3.2 μm as described in Section VII and in the text.

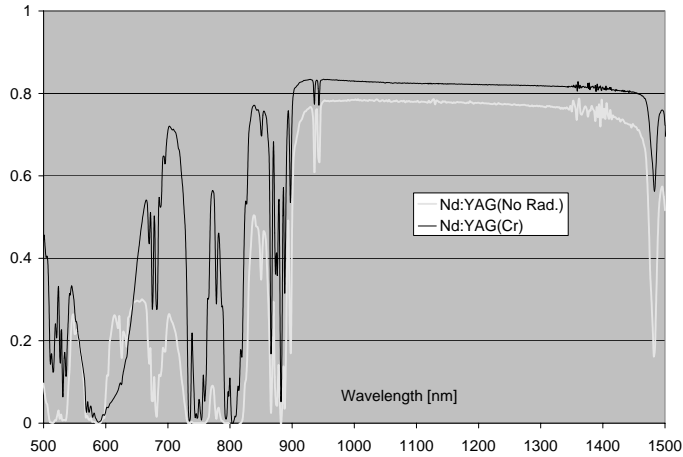


Fig. 7. Comparison of unirradiated transmission spectra for two differently doped YAG laser rods as described in the text.

IX. DISPERSIVE EFFECTS AND MATERIAL COMPARISONS

It is important to consider dispersion for different materials because of the especially short laser pulses that are important as well as the potentially long path lengths through the materials that may be required in the parallel, transmission mode. Fig. 10 shows some calculated curves over our typical wavelength range. These could be extended but were not because there was considerable dispersion in different results for certain materials. Examples are YAG and diamond that have impressive properties with important technical possibilities. Diamond (and Si) is an important covalent semiconductor so its dielectric properties are important but were only available in the visible and near UV e.g. an important, recent work[22] cites a single 1923 study that covers a narrow wavelength range. A similar and related statement can be made for dn/dT for a number of the materials considered here.

In Fig. 10, characteristic bands of materials are distinguished by a common crystal structure e.g. diamond and its equivalent binary compound - the zinc blende structure. The order within these two groups is correlated with their respective bandgap energies i.e. GaAs(1.42) and ZnSe(2.58) and for diamond (5.46), Si(1.12) and Ge(0.63). As discussed above, diamond was not plotted. An analytic relationship between n , $dn/d\lambda$ and E_G or

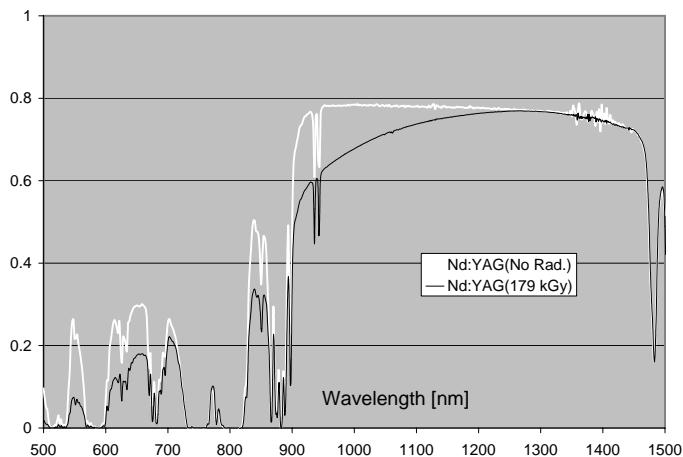


Fig. 8. Comparison for Nd:YAG rod after irradiation in Si equivalent dose.

crystal lattice constants could provide predictive possibilities. Above $2.5 \mu\text{m}$, Si is again preferred - especially considering earlier discussions and silicon's many practical advantages such as cost show a need for lasers near or above $2.5 \mu\text{m}$.

X. SUMMARY AND CONCLUSIONS

Although radiation damage is an important subject for high energy physics, our concerns are quite different from the usual ones in our field. These tend to be highly focused and rather piecemeal even though the field provides an array of interesting scientific problems.

Because we were interested in laser and optical materials, we began to study common glasses, including fused silica, since we expected these materials to be well understood because of their importance to the modern telecommunications industry. Our main interests were to find what was available, their general properties and to understand how different damage mechanisms changed or influenced these properties.

The subject is more complex and interesting than anticipated because distinguishing general properties from manufacturing characteristics is complicated by small variations in chemical composition, purity and fabrication procedures that often lead to large changes in response e.g. many materials can serve as detectors just as easily as windows depending solely on wavelength, impurities (or dopant) and defect concentration. To understand such characteristics our study has grown considerably.

We discussed a few aspects of high-energy colliders and accelerators that were relevant to damage mechanisms in conventional terms and related these to laser acceleration. While we were driven to this approach by the incredible advances in microelectronics and telecommunications that have been occurring, the need to integrate these is clear and the potential fallout is large[6]. Perhaps the only essential difference between what we are trying to do and industry is based on the need for extremely radiation resistant materials. However, if these can be developed in a natural way at a reasonable cost then it should benefit everyone.

We obtained results for a broad array of materials including a range of characteristics for many of them. Examples include differing thicknesses of quartz, Si, a-SiO₂, GaAs, Al₂O₃, Ti:Sa,

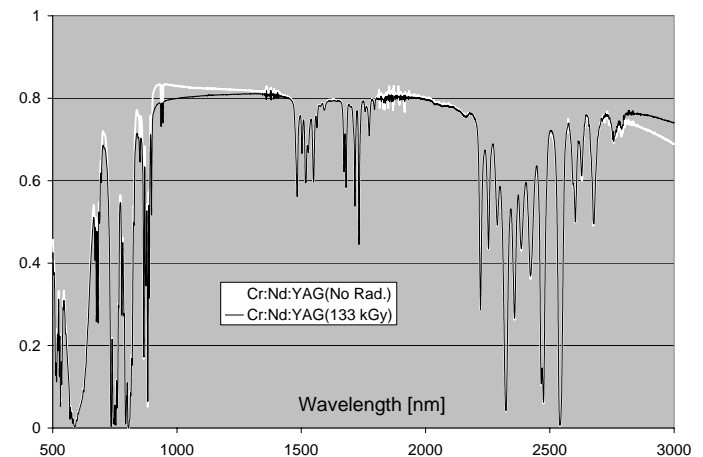


Fig. 9. Comparison for Cr:Nd:YAG rod after irradiation in Si equivalent dose.

YAG, diamond, LiNbO_3 , CaF_2 , MgF_2 and a number of different glasses and dopings of Nd:YAG. The variations in response are remarkable. Fortunately, the quartz and silicon appear quite acceptable, as are the fluorides, at current levels of dose, if we do not go above their long wavelength cutoffs.

MgF_2 is a better window material than Sapphire or YAG and CaF_2 , a cubic, is even better reaching up to nearly $10\ \mu\text{m}$ but ZnSe runs up to $20\ \mu\text{m}$ and for related reasons is a potential laser candidate[23]. CaF_2 is especially noteworthy having the highest laser damage threshold ($> 2.2\ \text{J}/\text{cm}^2$) with little to no difference between air and vacuum. Its transmission spectrum is quite flat and $> 90\%$ from 0.8 - $3.2\ \mu\text{m}$ with no water evident. We have seen no radiation damage in any fluoride sample but measurements are ongoing. Their dispersions are also lower than all materials except ZnSe .

Diffusion of water and hydrogen into silica leads to silanol and hydride groups that enhance the lowest absorption bands and restricts the use of silica and quartz. It is interesting that diamond and Al_2O_3 show quite flat transmission but both show an effect at $670\ \text{nm}$ [19]. The most important result may be that Si appears to be ideal except possibly with CO_2 lasers. Although we have used it under full electron beams, we have yet to do the laser damage tests because of its unfavorable bandgap at typical laser wavelengths that are available (Ti:Sa and Nd:YAG). These will be done and we are also beginning tests on ZnSe and ZnTe .

Clearly, neutron displacement studies are of interest both for Si but also for differences between a- and c- SiO_2 as well as the other crystalline materials discussed here. Doping, impurities and fabrication procedures add very large complications - presumably because they begin to lower the Fermi level to that of the defects that may be mobile and can take many forms. However, presently, it seems clear that pure amorphous materials are preferred over typical glasses and that pure crystalline materials are preferred over the pure amorphous because of their greater number of states and structural characteristics such as greater susceptibility to permeation. It will be interesting to see whether these conclusions remain after neutron displacement studies that are now being pursued with both fast and slow, pure neutron sources.

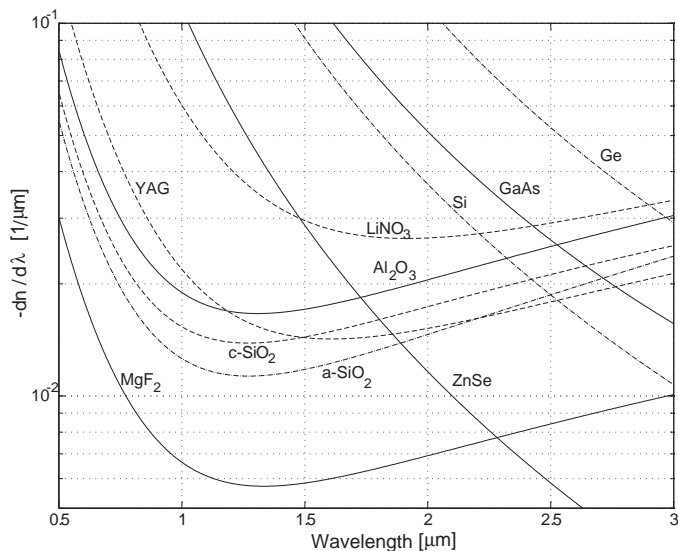


Fig. 10. Representative dispersion curves calculated for materials of interest.

ACKNOWLEDGMENTS

We would like to thank several people who have contributed to this project. Frederick Bourgeois and Roger Route, in Bob Byer's Group at Stanford, were instrumental to our use of the Hitachi Spectrophotometer as well as providing some samples. George Marcus introduced us to the Bruker FTIR at Stanford's HEPL. Rahul Prasad of Alameda Applied Sciences Corp. provided several natural diamond samples. Stan Mao facilitated the connection with Lockheed Martin and SLAC's Physical Electronics Group provided great support.

REFERENCES

- [1] R.T. Williams and E.J. Friebele, *CRC Handbook of Laser Science and Technology*, vol. III, CRC Press, Boca Raton, 1986.
- [2] Kyle B. Miller, James Leitch and Chandra Lyons-Mandel, "Proton radiation testing of optical elements", *NSREC Proc.*, pp. 155-159, 2001.
- [3] H. Henschel, O. Kohn, "Regeneration of irradiated optical fibres by photobleaching? ", *IEEE Trans. on Nucl. Sci.*, vol. 47 pp. 699-704, 2000.
- [4] Y.C. Huang et al, "The physics experiment for a laser-driven electron accelerator", *Nucl. Inst. Meth.*, A407, pp. 316-321, 1998.
- [5] T. Plettner et al, "Status of the laser electron accelerator project (LEAP)", *Quantum Aspects of Beam Physics*, World Scient. Publ. Co., Singapore, pp. 310-321, 1999.
- [6] J. E. Spencer, "The silicon lattice accelerator," *Int'l Jnl. Mod. Phys. A*, To be published, December 2002.
- [7] M. Stanley Livingston and John P. Blewett, *Particle Accelerators*, McGraw-Hill, New York, 1962. Most recently see: Maury Tigner, "Does accelerator-based particle physics have a future", *Phys. Today* vol. 54, Jan. 2001.
- [8] J.E. Spencer, "Beam-Beam effects and generalized luminosity", *Int'l Jnl. Mod. Phys. A*, vol. 11, pp. 1675-1687, 1996.
- [9] J.E. Spencer, "Limitations imposed by beam-beam effects and their remedies", *Int'l Jnl. Mod. Phys. A*, vol. 13, pp. 2479-2492, 1998.
- [10] J. E. Spencer, "Limitations imposed by beam-beam effects and their remedies - II", *Int'l Jnl. Mod. Phys. A*, vol. 15, pp. 2543-2554, 2000.
- [11] M. D. Perry, B. C. Stuart, P. S. Banks, M. D. Feit, V. Yanovsky, and A. M. Rubenchik, "Ultrashort pulse laser machining of dielectric materials", *J. Appl. Phys.*, vol. 65, pp. 6803-6810, 1999.
- [12] Power sources are presently available that could provide higher gradients than RF with 50 MHz rep rates e.g. see the IMRA America, Inc. website.
- [13] The standard means for producing ingots of monocrystalline Si is the Czochralski (Cz) technique for which there appears to be no correlation between transmissivity and conductivity.
- [14] Chris B. Schaffer, Andre Brodeur and Eric Mazur, "Laser-Induced breakdown and damage in bulk transparent materials induced by tightly focused femtosecond laser pulses", *Meas. Sci. Technol.*, vol. 12, pp. 1784-1792, 2001.
- [15] T.R. Oldham, "Analysis of damage in MOS devices for several radiation environments", *IEEE Trans. on Nucl. Sci.*, vol. 31 pp. 1236-1241, 1984.
- [16] UV grade, fused silica from CVI Laser Corp. was made by flame hydrolysis of silicon tetrachloride (SiCl_4) (Part# RAP-50-UV).
- [17] Lithosil is a trademark of Schott Lithotec AG with ≤ 0.05 PPM of both Al and Na impurities. We have been unable to obtain this material. Infrasil 301 is a fused quartz product of CVI of interest with < 10 PPM of OH. A "wet" silica is also of interest.
- [18] B. Brichard, A. Fernandez Fernandez, F. Berghmans, M. Decretton, "Origin of the radiation-induced OH vibration band in polymer-coated optical fibres", *IEEE Trans. on Nucl. Sci.*, 2002, This issue.
- [19] T. Bakos, A.N. Rashkeev and S. T. Pantelides, "The origin of Photoluminescence lines in irradiated Amorphous SiO_2 ", *IEEE Trans. on Nucl. Sci.*, 2002, This issue.
- [20] P. E. Bunson, M. Di Ventra, S. T. Pantelides, D. M. Fleetwood, and R. D. Schrimpf, "Hydrogen-related defects in irradiated SiO_2 ", *IEEE Trans. on Nucl. Sci.*, vol. 47 pp. 2289-2296, 2000.
- [21] T.S. Rose, M.S. Hopkins and R.A. Fields, "Characterization and control of gamma and proton radiation effects on the performance of Nd:YAG and Nd:YLF lasers", *IEEE J. Quant. El.*, vol. 31, pp. 1593-1602, 1995.
- [22] R.W. Wayant and M.N. Ediger, *Electro-Optics Handbook*, McGraw Hill, New York, 1994.
- [23] Irina T. Sorokina and Evgeni Sorokin; Alberto Di Lieto and Mauro Tonelli; Ralph H. Page and Kathleen I. Schaffers, "Efficient broadly tunable continuous-wave $\text{Cr}^{2+}:\text{ZnSe}$ laser", *J. Opt. Soc. Am.*, vol. 18, pp. 926-930, 2001.